




Cite this: *Nanoscale*, 2018, **10**, 6147

Mesoporous-silica induced doped carbon nanotube growth from metal–organic frameworks†

Huang Zhou,^a Daping He,^{*a,b} Amiin Ibrahim Saana,^a Jinlong Yang,^a Zhe Wang,^a Jian Zhang,^a Qirui Liang,^a Shuai Yuan,^a Jiawei Zhu^a and Shichun Mu[†]  ^{*a}

Carbon materials, with a controllable structure, derived from metal–organic frameworks (MOFs) have emerged as a new class of electrocatalysts in renewable energy devices. However, efficient conversion of MOFs to small diameter doped carbon nanotubes in inert gases at high temperatures (>600 °C) remains a significant challenge. In this study, we first report the growth of small diameter cobalt and nitrogen co-doped carbon nanotubes (Co/N-CNTs) from mesoporous silica (mSiO₂)-coated Co-based MOFs (ZIF-67). The presence of a layer of mSiO₂ outside the ZIF-67 nanocrystals prevents the Co nanocatalysts from quick aggregation, and significantly serves as a unique ‘sieve’ for inducing the catalytic growth of CNTs during pyrolysis. The obtained Co/N-CNTs, with ~13 nm diameter evolved from the pristine MOF architecture, exhibit higher catalytic activity and stability for oxygen reduction than commercial Pt/C electrocatalysts in alkaline media. This novel strategy opens a new avenue for the synthesis of Co/N-CNTs with great promise for developing high performance and cheap electrocatalysts.

Received 6th January 2018,
Accepted 22nd February 2018

DOI: 10.1039/c8nr00137e

rsc.li/nanoscale

1. Introduction

The electrochemical oxygen reduction reaction (ORR) is a crucial step for electrochemical energy storage and conversion technologies, including proton exchange membrane fuel cells (PEMFCs), alkaline fuel cells (AFCs), direct methanol fuel cells (DMFCs) and metal–air batteries.^{1,2} However, low activity and unstable oxygen reduction catalysts are a major barrier to building such electrochemical energy devices. Pt-Based materials have been proven to be the most efficient ORR catalysts,³ but the high cost, scarcity, instability, and poor methanol (CH₃OH) and carbon monoxide (CO) tolerance are big obstacles for large-scale application of Pt-based catalysts.^{4,5} Considerable efforts have been devoted to exploring non-precious-metal based or metal-free catalysts. Among them, metal and nitrogen co-doped carbon materials (M/N-C),^{6–14} especially M/N co-doped carbon nanotubes (M/N-CNTs), have been widely studied as promising candidates owing to their extraordinary electronic and novel structural properties.

Although strategies for the synthesis of M/N-CNTs have been developed quickly, it is still a great challenge to develop a highly efficient and easily scalable method for M/N-CNT growth.

In recent years, owing to the unique carbon and nitrogen-rich organic components and fascinating porous architectures, the pyrolysis of metal–organic frameworks (MOFs) has emerged as a new efficient strategy for the synthesis of various M/N-C materials.^{5,7,15–20} One of the emerging hot topics is to obtain M/N-CNTs from MOFs. In 2016, Lou *et al.* reported that the N and cobalt Co carbon nanotubes (Co/N-CNTs) in hollow frameworks can be synthesized by pyrolysis of a Co-based zeolitic imidazolate framework (ZIF-67) in Ar/H₂ gas. And as electrocatalysts, such Co/N-CNTs exhibit high activity and stability in the ORR and oxygen evolution reaction (OER).⁸ Very recently, Mai *et al.*²¹ developed a low-temperature and slow pyrolysis strategy for the synthesis of Co/N-CNTs from selected MOFs (435 °C, 8 h). After a subsequent higher temperature (700 °C) treatment, the doped CNTs show better ORR activity than that of Pt/C catalysts.²¹ It is found that by either using a H₂ reduction agent or slow pyrolysis at low temperatures, small nanocatalysts with high activity can be obtained, which play a vital role in the CNT growth from MOF materials during the heating process. However, the efficient transformation of MOFs to small diameter M/N-CNTs at a high temperature (>600 °C) in an inert gas is still a huge challenge and highly desired.

^aState Key Laboratory of Advanced Technology for Materials Synthesis and Processing, Wuhan University of Technology, Wuhan 430070, China.
E-mail: msc@whut.edu.cn, hedaping@whut.edu.cn

^bHubei Engineering Research Center of RF-Microwave Technology and Application, School of Science, Wuhan University of Technology, Wuhan 430070, China

†Electronic supplementary information (ESI) available. See DOI: 10.1039/c8nr00137e

Herein, we report a successful controllable synthesis of MOF derived Co/N-CNTs with a small diameter (~13 nm) by using mesoporous-silica (mSiO₂) layer (as 'sieves') covered ZIF-67 nanocrystals (as the precursor). During the high-temperature pyrolysis, the coated mSiO₂ shell not only prevents Co nanoparticles from rapid aggregation in the internal of ZIF-67, resulting in the formation of small Co nanocatalysts with high activity, but also provides unique external 'sieves' to induce the catalytic growth of CNTs. The as-prepared Co/N-CNTs possess a 3D network structure, high nitrogen-doping level, and optimum graphitic degree, which confer excellent ORR activity, stability and CH₃OH tolerance, thereby offering huge potential to replace Pt/C catalysts for large-scale applications. To the best of our knowledge, this cheap strategy has not yet been applied to fabricate MOF-derived M/N-CNTs during high temperature annealing.

2. Experimental

Materials and reagents

Analytical grade cobalt nitrate hexahydrate (Co(NO₃)₂·6H₂O), 2-methyl imidazole (MeIM), NaOH, cetyltrimethylammonium bromide (CTAB) and tetraethyl orthosilicate (TEOs) were obtained from Shanghai Chemical Reagents, China. The commercial Pt/C catalyst is 20 wt% of ~3 nm Pt nanoparticles on a Vulcan XC-72 carbon support. Nafion was acquired from Sigma-Aldrich. All of the chemicals used in this experiment were analytical grade and used without further purification.

Preparation of ZIF-67 crystals

All chemicals and solvents were purchased from commercial sources and used without purification. In a typical procedure, Co(NO₃)₂·2.6H₂O (1.092 g) was dissolved in 30 mL of methanol and then injected into 30 mL of methanol containing 1.232 g of 2-methylimidazole (MeIM) with sonication for 5 minutes at room temperature. Then, the resulting solution was stirred at room temperature for 4 h. The as-obtained precipitates were centrifuged and washed with methanol several times and dried under vacuum at 70 °C overnight.

Preparation of Co NPs/N-C

The carbonized products were synthesized by the pyrolysis of ZIF-67 at 700 °C for 3 h under N₂ gas, followed by slow cooling to room temperature. The heating rate was 5 °C min⁻¹.

Preparation of ZIF-67@mSiO₂

ZIF-67 (400 mg) was dispersed in 160 mL of H₂O, and then 5 mL of aqueous cetyltrimethylammonium bromide (CTAB) solution (20 mg mL⁻¹) and 6.4 mL of aqueous NaOH solution (6 mg mL⁻¹) were added under sonication for 5 min at room temperature to form a uniform solution. Subsequently, different volumes of tetraethyl orthosilicate (TEOs) solution (0.08, 0.4, 0.8 or 1.2 mL in 4 mL of methanol) were injected into the above solution, respectively, and stirred for 0.5 h. The resulting ZIF-67@mSiO₂ core-shell nanoparticles with

different masses of SiO₂ coating were centrifuged and washed several times with ethanol and dried under vacuum at 70 °C overnight.

Preparation of Co/N-CNTs

Co/N-CNT products were synthesized by the pyrolysis of ZIF-67@mSiO₂ core-shell nanoparticles (0.4 mL TEOs was used for mSiO₂ coating) at 700 °C for 3 h under N₂ gas, followed by slow cooling to room temperature. The heating rate was 5 °C min⁻¹. To remove the mSiO₂ shell, pyrolyzed samples were immersed in aqueous HF (10 wt%) at 80 °C for 6 h, followed by centrifugation and washing with deionized water and ethanol, and drying under vacuum at 70 °C overnight. The products were denoted as Co/N-CNTs-*x* and were synthesized by similar procedures to Co/N-CNTs, where *x* = 1, 5, 10, and 15 represent the mass of mSiO₂ in grams, corresponding to different volumes of TEO solution (0.08, 0.4, 0.8 and 1.2 mL).

Characterization

The field-emission scanning electron microscopy (FESEM) images were obtained by using a Hitachi S-4800 microscope with an accelerating voltage of 20 kV. Elemental mapping was performed using an energy-dispersive X-ray spectroscope attached to the Hitachi S-4800 transmission electron microscopy (TEM) and high resolution TEM (HRTEM) images were obtained by using a JEM-2100F microscope with an accelerating voltage of 200 kV. High-angle annular dark-field scanning transmission electron microscopy energy dispersive spectrometer (HAADF-STEM-EDS) element mappings were carried out on a Titan G2 60-300. X-ray diffraction (XRD) patterns were recorded on an X-ray D/Max-RB instrument by using Cu-Kα radiation. Raman shifts were carried out by using a LabRAM Aramis Raman spectrometer instrument with an excitation wavelength of 633 nm using the Ar ion laser. X-ray photoelectron spectroscopy (XPS, VG-Multilab2000) was performed by using Al Kα radiation (1486.71 eV). The nitrogen sorption experiments were performed at 77 K on a Micromeritics ASAP 2020 system. Prior to the experiments, the samples were degassed under vacuum at 300 °C for 12 h. The Scherrer's law is:

$$D = K\lambda/B \cos \theta$$

where *D* denotes the nanoparticle size, *K* is Scherrer constant (0.89), *λ* is the X-ray wavelength (0.15406 nm), *B* is the half peak width, and *θ* is the X-ray diffraction angle.

Electrochemical measurements

Electrochemical evaluation was conducted at room temperature on a CHI 660E electrochemical workstation. A rotating disk electrode (RDE) with a glassy carbon (GC) disk was used as a working electrode (5 mm in diameter). The Pt wire and Ag/AgCl were used as the counter and reference electrodes, respectively. To prepare the catalyst ink, 5 mg catalyst powder was ultrasonically dispersed in 500 μL mixed liquor (25 μL Nafion ionomer solution and 475 μL isopropanol). The working electrode was prepared by loading 0.30 mg cm⁻² of

the catalyst and commercial Pt/C (20 wt%, Johnson Matthey Corp.), as a benchmark, was kept at 15 $\mu\text{g Pt per cm}^2$. All ORR measurements were conducted in O₂-saturated 0.1 M KOH solution. Cyclic voltammetry (CV) measurements were carried out over the potential range of -1.0 to $+0.2$ V with a scan rate of 20 mV s^{-1} . The linear sweep voltammetry (LSV) measurements were recorded over the potential range of -0.9 to -0.2 V at different rotation rates with a scan rate of 10 mV s^{-1} . The stability of the catalyst was evaluated by current *vs.* time ($-t$) chronoamperometric response during a constant potential of -0.35 V at a rotation rate of 1600 rpm. The CH₃OH (1 M) and CO ($V_{\text{CO}}/V_{\text{O}_2} \approx 10\%$) tolerance tests were evaluated during a constant potential of -0.5 V at a rotation rate of 1600 rpm.

The kinetic parameters can be calculated based on the Koutecky–Levich (K–L) equations as follows:

$$\frac{1}{J} = \frac{1}{J_L} + \frac{1}{J_K} = \frac{1}{B\omega^{1/2}} + \frac{1}{J_K} \quad (1)$$

$$B = 0.62nFC_0(D_0)^{2/3}(\nu)^{-1/6} \quad (2)$$

where J denotes the measured current density, J_K is the kinetic current density of the ORR, J_L is the diffusion-limited current density, F is the Faraday constant (96,485 C mol⁻¹), C_0 is the bulk concentration of O₂ (1.26×10^{-3} mol L⁻¹), D_0 is the O₂ diffusion coefficient in 0.1 mol L⁻¹ KOH, ν is the kinetic viscosity of the solution (1.09×10^{-2} cm² s⁻¹) and ω is the electrode rotation rate (rps).

3. Results and discussion

The strategy for synthesizing Co/N-CNTs is schematically depicted in Fig. 1a. In the first step, the well-defined ZIF-67 was synthesized by employing cobalt ions as a metallic node, 2-methylimidazole as an organic linker, and methanol as a solvent.²² As shown in the FESEM images (Fig. 1b and Fig. S1†) and TEM images (Fig. 1e and Fig. S2†), the as-prepared ZIF-67 crystals show a typical dodecahedral shape with a smooth surface and an average particle size of ~ 600 nm (the particle-size distribution is shown in Fig. S2c†). Then, a mesoporous silica (mSiO₂) shell is coated onto the surface of ZIF-67 dodecahedra by using NaOH to catalyze the hydrolysis of TEOs and CTAB as the pore-generating agent.^{23–26} The obtained ZIF-67@mSiO₂ investigated by FESEM observation (Fig. 1c) retains the dodecahedral shape with a rough mSiO₂ coating layer. Such a morphological feature is also evidenced by the TEM images (Fig. 1f). The high-resolution TEM image (HR-TEM) at the edge of ZIF-67@mSiO₂ in Fig. S3b† clearly illustrates the presence of a large amount of uniformly distributed mesopores, and the pore diameter is estimated to be ~ 3 nm. The corresponding nitrogen adsorption–desorption isotherms further confirm the existence of mesopores (Fig. S3c†), as the hysteresis loop shows a typical type H₄ isotherm.²⁷ The pore size distribution curve (Fig. S3d†) exhibits a distinct peak centered at 3 nm, which is totally different from the curve of ZIF-67 (Fig. S4†) and agrees well with the HR-TEM results. Finally, after being annealed in a furnace under flowing nitrogen gas (N₂), the clean Co/N-CNTs assembled to a

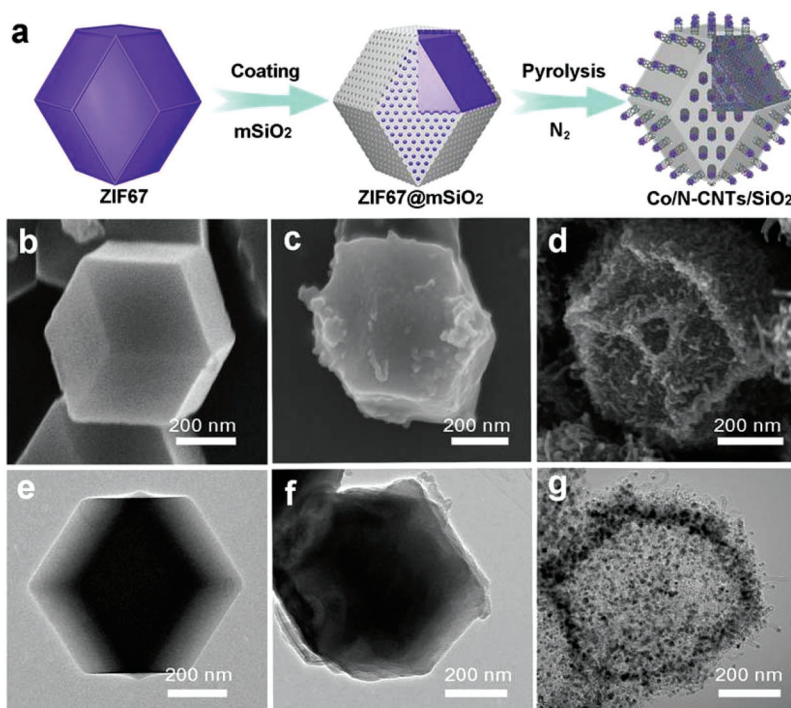


Fig. 1 (a) Synthetic procedure of the Co/N-CNTs by the mSiO₂ coated calcination strategy. (b–d) FESEM and (e–g) TEM images of the as-prepared ZIF-67, ZIF-67@mSiO₂ and Co/N-CNTs.

well-retained dodecahedra structure (Fig. 1d and g, and Fig. S5†) is obtained by the removal of the mSiO₂ layer in light of etching.

The detailed structure of Co/N-CNTs was detected by HR-TEM and high-angle annular dark-field scanning TEM (HAADF-STEM). Fig. 2a and b reveal the Co/N-CNTs with a well retained dodecahedra shape, and homogeneous distribution of C, N, O and Co (as seen in HAADF-STEM EDS element mapping images). Fig. 2c further reveals that a single CNT with ~13 nm diameter is multiwalled with distinct lattice fringes and a *d*-spacing of ~0.35 nm, corresponding to the (002) diffraction plane of graphitic carbon.⁹ The Co nanoparticle is encapsulated by few layered graphitic carbons at the tip of the CNT. HAADF-STEM EDS element mapping analysis (Fig. 2d) reveals that the Co element only concentrates on the tip of the nanotube, whereas C, N, and O elements are uniformly distributed over the entire CNT (a single CNT with Co removed by HF in Fig. S6† further reveals that C, N, and O elements are uniformly distributed). Furthermore, it is important to point out that the HRTEM images of Co/N-CNTs show that all the CNTs have a diameter of ~13 nm (Fig. 2e and f).

The X-ray diffraction (XRD) pattern of Co/N-CNTs shows only two peaks (Fig. 2g), in which the broad peak (~26°) indexes the (002) plane of graphitic carbon and the narrow

peak (~44.3°) corresponds to the Co (111) phase. According to Scherrer's law, the diameter of Co nanoparticles was calculated to be 10.81 nm, which is slightly lower than the nanotube diameter (~13 nm). The X-ray photoelectron spectroscopy (XPS) survey spectrum further confirms the presence of C, N, O, and Co, with the atomic ratio of 86.87, 6.56, 5.71 and 0.86%, respectively (Fig. 2h). The high-resolution N 1s spectrum (Fig. 2i and Fig. S7†) can be further deconvoluted into two sub-peaks of nitrogen species at 398.7 and 400.9 eV, corresponding to the pyridinic N atom and the graphitic N atom,⁹ respectively. In agreement with the implications of XPS for N 1s, the XPS spectrum in the Co region of Co/N-CNTs shows two sub-peaks with binding energies of 779.4 eV and 793.5 eV, corresponding to the Co 2p_{3/2} and Co 2p_{1/2} levels, respectively (Fig. S8†). Raman Spectroscopy was used to further investigate the carbon structure of Co/N-CNTs at different pyrolysis temperatures (Fig. S9†), in which two peaks at 1335 and 1587 cm⁻¹ indicate the existence of disordered sp³ carbon or defected carbon (D-band) and graphite sp² carbon (G-band),^{28,29} respectively. The intensity ratio of the D band to G band (*I*_D/*I*_G) calculated to be ~0.97 for Co/N-CNT pyrolysis at 700 °C is lower than that of Co NP/N-C (1.12) synthesized at the same temperature (Fig. S10†), which can be attributed to the formation of more graphitic carbon in Co/N-CNTs. The N₂

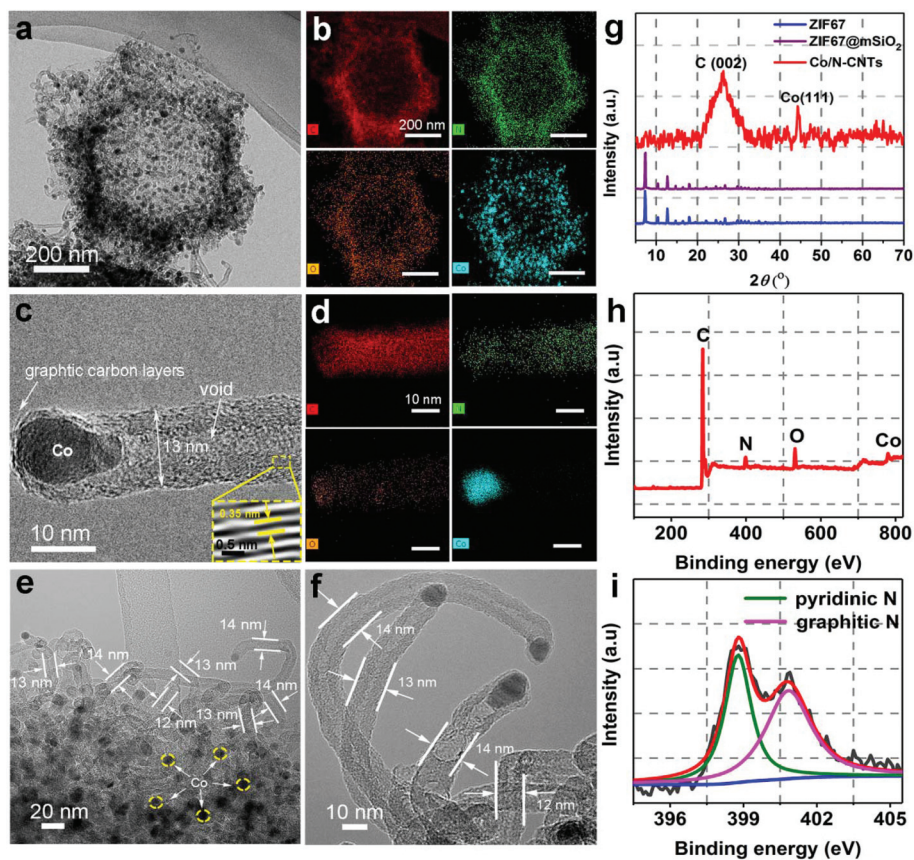


Fig. 2 TEM images of (a) Co/N-CNTs and (c) a single Co/N-CNT, and the corresponding EDS mapping images (b) and (d). (c) XRD patterns of the as-prepared ZIF-67, ZIF-67@mSiO₂ and Co/N-CNTs. (h) XPS spectra of Co/N-CNTs, the inset figure is the N 1s XPS spectra.

adsorption-desorption isotherms of Co/N-CNTs are shown in Fig. S11,† a type H₄ hysteresis loop indicates the existence of mesopores, and the pore-size distribution analysis by the Barrett-Joyner-Halenda method reveals the mesoporosity of Co/N-CNTs with relatively wide pore-size distribution in the range of 2–10 nm.

The highly active nitrogen-doping level, rich mesopores and graphitic carbon structure of Co/N-CNTs make it a promising ORR catalyst for fuel cells and metal-air batteries. Therefore, the catalytic properties were probed by cyclic voltammetry (CV) on a rotating disk electrode (RDE) in O₂-saturated 0.1 M KOH solution. For comparison, Co-NP/N-C and commercial Pt/C were also tested. As shown in Fig. 3a, Co/N-CNTs exhibit a well-defined oxygen reduction peak centered at -0.176 V vs. Ag/AgCl. The ORR performance was further investigated by linear sweep voltammetry (LSV) in O₂-saturated 0.1 M KOH solution. As shown in Fig. 3b, Co/N-CNTs exhibit the best ORR catalytic activity among the three catalysts, as judged by the onset potential (E_0), half-wave potential ($E_{1/2}$) and limiting current density (j). Typically, the E_0 of Co/N-CNTs is the same as that of Pt/C (-0.005 V), while its $E_{1/2}$ and j ($E_{1/2} = -0.154$ V, $j = 5.82$ mA cm⁻²) show 21 mV more positive and 0.40 mA cm⁻² larger than those of Pt/C ($E_{1/2} = -0.175$ V, $j = 5.42$ mA cm⁻²), and also superior to that of Co NP/N-C ($E_0 = -0.063$ V, $E_{1/2} = -0.222$ V, $j = 4.26$ mA cm⁻²) and most of the reported non-

precious top electrocatalysts (ESI, Table S1†). The Tafel plot of Co/N-CNTs (83 mV dec⁻¹) is also slightly lower than that of Pt/C (92 mV dec⁻¹), further confirming the excellent ORR activity (Fig. 3c).¹⁷ Furthermore, the Koutecky-Levich plots of Co/N-CNTs obtained from RDE polarization curves at various rotating speeds (Fig. 3d) exhibit a good parallel linear relationship from -0.3 to -0.7 V, suggesting first-order reaction kinetics for ORR.^{8,30,31} The average electron transfer number is calculated to be *ca.* ~3.89, demonstrating a four electron ORR pathway.

Moreover, the current density of Co/N-CNTs shows a negligible decay of only ~3% after 22 000 s *i-t* chronoamperometric analysis, whereas Pt/C shows a loss of ~14%, suggesting a superior stability of the Co/N-CNTs (Fig. 3e). This high stability was further confirmed by the much smaller decay of the half-wave potential before and after the *i-t* test for Co/N-CNTs (~2 mV) compared to Pt/C (~19 mV) (Fig. S12†). The stability was also measured by *i-t* response in the presence of methanol and CO. As shown in Fig. 3f, Co/N-CNTs show only ~2% current density decay after 200 s upon injecting methanol (1 M), however, the current density of the Pt/C catalyst decays by ~13%. Similarly, Pt/C suffers a more serious CO poisoning effect ($V_{CO}/V_{O_2} \sim 10\%$) as judged by the current density decay after 200 s (~7%) than that of Co/N-CNTs (~2%) (Fig. S13†). These results reveal that Co/N-CNTs with high catalytic activity

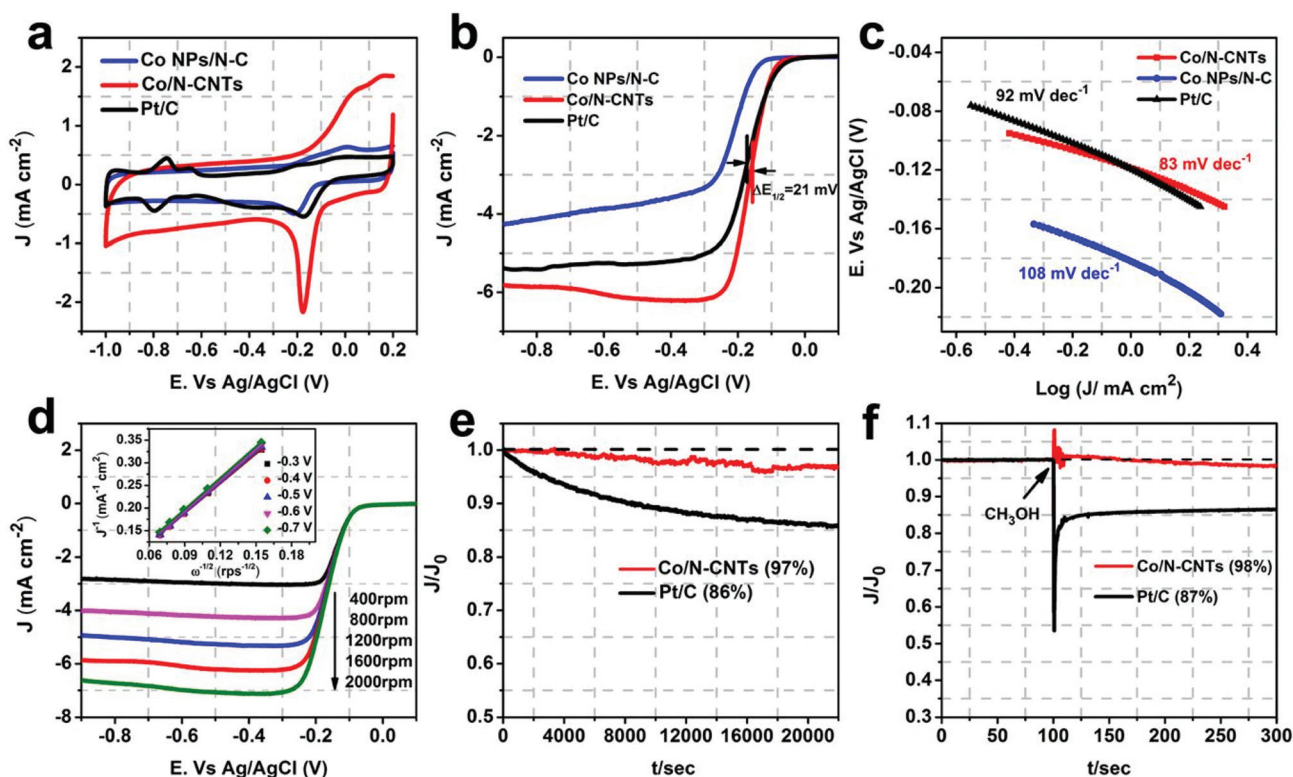


Fig. 3 (a) CV curves, (b) LSV curves and (c) Tafel plots of Co/N-CNTs, Co NPs/N-C and Pt/C. (d) LSV curves of Co/N-CNTs at different rotation rates with a scan rate of 10 mV s⁻¹ and the corresponding K-L plots (inset) at different electrode potentials from -0.3 V to -0.7 V. The current vs. time (*i-t*) chronoamperometric responses of Co/N-CNTs and Pt/C: (e) was recorded at a constant potential at -0.35 V and (f) was recorded at a constant potential at -0.5 V.

also have a significantly superior catalytic stability and immunity to methanol crossover and CO poisoning, indicating a promising alternative to the Pt/C catalyst.

Fig. 4 provides a schematic illustration of the Co nanoparticles and CNT evolution from the ZIF-67 nanocrystal with or without the mSiO₂ ‘sieve’ during pyrolysis, thereby providing an intrinsic understanding of the formation mechanism of the Co/N-CNTs. As shown in Fig. S14a,† with the use of bare ZIF-67 (without any mSiO₂ coating) as a precursor, the Co-ions within the ZIF-67 framework are firstly converted into a uniform Co nanoparticle wrapped polymer (2-methylimidazole clusters) during the heat treatment (Fig. 15c†).²¹ When the temperature further increases, the Co nanoparticles aggregate quickly without any hindrance while the polymer scaffold is transformed into carbon layers (Co NP/N-C, as evidenced by the FESEM images in Fig. S14b and c,† and previous work³²). With ZIF-67@mSiO₂ as a precursor (Fig. 4), the first step is similar to the formation of Co NP/N-C, wherein the Co-ions within the ZIF-67@mSiO₂ are first converted into uniform Co nanoparticles at low temperatures (Fig. S15a†).³³ However, the small Co nanoparticles can be maintained even at high temperatures due to the protection of the mSiO₂ layer. The diameters of Co nanoparticles in ZIF-67@mSiO₂ are small (2–3 nm) even at a temperature up to 580 °C (Fig. S15b†), which is much smaller than the diameter of Co nanoparticles of ZIF-67 without the protection of mSiO₂ at the same temperature (Fig. S15c†). As shown in Fig. S16a,† the Co nanoparticles wrapped by carbon layers are small and located on the dodecahedra surface even when the ZIF-67@mSiO₂ is heated at 600 °C for 3 h. When the temperature increases to 650 °C, a large amount of Co nanoparticles wrapped by carbon

layers and short CNTs on dodecahedra surfaces emerge (Fig. S16b and c†). In the barrier-free environment and at higher temperature, the Co nanoparticles on the tip of the CNTs drive the nanotubes to be longer. As shown in Fig. S16d,† the well-defined hollow structure dodecahedral assembled by Co and N co-doped CNTs (Co/N-CNTs) can be obtained after ZIF-67@mSiO₂ is heated at 700 °C, which may be due to the preferential control of the Co NP size effective near the mSiO₂ shell, and hence the CNT growth occurs in the mSiO₂ shell, leading to such a hollow shape. However, when the temperature rises to 800 and 900 °C (Fig. S16e and f†), the dodecahedra framework becomes much rougher with longer CNTs and more serious aggregation of the Co nanoparticles.

To further understand the effect of mesopores of the SiO₂ shell on the CNT growth, ZIF-67 crystals with different mass ratios of mSiO₂ coating in the range of 1 to 15 were pyrolyzed under a N₂ atmosphere at 700 °C and etched with HF (denoted as Co/N-CNTs-x). The sample obtained with the lowest mass of mSiO₂ (Co/N-CNTs-1), in the FESEM image (Fig. S17a†), shows a dodecahedral shape with many Co nanoparticles and few short CNTs on the surface. With the increase of mSiO₂, Co/N-CNTs-5 shows dodecahedral frameworks with rougher surfaces and more nanotube frameworks (Fig. S17b†). However, when the amount of mSiO₂ coated on the ZIF-67 continuously increased, as shown in the FESEM images in Fig. S17c and d,† the quantity of Co/N-CNTs-10 and Co/N-CNTs-15 shows a diminished trend, which is due to that the mSiO₂ shell with poor mesoporous structures is too thick to hinder the growth of nanotubes. Consequently, the formation and growth of the Co/N-CNTs can be well controlled by simply regulating the optimum amount of mSiO₂ coatings.



Fig. 4 Formation mechanism of Co/N-CNTs.

4. Conclusions

In summary, with mSiO₂ coated on the ZIF-67 nanocrystal surface, we have successfully synthesized carbon nanotubes co-doped with Co and N through a pyrolysis method. The as-prepared Co/N-CNTs with a robust 3D framework structure possess excellent ORR activity, stability and CH₃OH tolerance, even superior to commercial Pt/C electrocatalysts in alkaline media. The oriented formation mechanism was firstly revealed by further analyzing the effect of the mSiO₂ shell during the high-temperature pyrolysis. The mSiO₂ shell not only confines the Co nanoparticles from undesirable fusion, but also provides a novel external passageway which induces the catalytic nanoparticle transmission and growth of CNTs. This 'sieve' controllable strategy yields Co/N-CNT products with a high specific surface area and oriented CNT-assembled architecture, and further allows good control over the CNT diameter. Undoubtedly, this research opens up a new avenue for synthesis of novel MOF-derived carbon nanotubes and provides new cheap candidates as noble metal based electrocatalysts in renewable energy technologies.

Conflicts of interest

There are no conflicts to declare.

Acknowledgements

This work was supported by the National Natural Science Foundation of China (51372186, 51672204, 51701146). We also acknowledge the Center for Materials Research and Analysis of Wuhan University of Technology for HR-TEM (Yi Guo) and friends (Sijia Wu, Lijia Qu) for SEM tests and picture suggestions.

Notes and references

- 1 J. Suntivich, H. A. Gasteiger, N. Yabuuchi, H. Nakanishi, J. B. Goodenough and Y. Shao-Horn, *Nat. Chem.*, 2011, **3**, 546–552.
- 2 D. He, H. Tang, Z. Kou, M. Pan, X. Sun, J. Zhang and S. Mu, *Adv. Mater.*, 2017, **29**, 1601741.
- 3 E. Proietti, F. Jaouen, M. Lefèvre, N. Larouche, J. Tian, J. Herranz and J. P. Dodelet, *Nat. Commun.*, 2010, **2**, 416.
- 4 Y. C. Wang, Y. J. Lai, L. Song, Z. Y. Zhou, J. G. Liu, Q. Wang, X. D. Yang, C. Chen, W. Shi and Y. P. Zheng, *Angew. Chem., Int. Ed.*, 2015, **54**, 9907–9910.
- 5 Y. Chen, S. Ji, Y. Wang, J. Dong, W. Chen, Z. Li, R. Shen, L. Zheng, Z. Zhuang and D. Wang, *Angew. Chem., Int. Ed.*, 2017, **56**, 6937–6941.
- 6 V. Armel, S. Hindocha, F. Salles, S. Bennett, D. Jones and F. Jaouen, *J. Am. Chem. Soc.*, 2017, **139**, 453–464.
- 7 L. Shang, H. Yu, X. Huang, T. Bian, R. Shi, Y. Zhao, G. I. Waterhouse, L. Z. Wu, C. H. Tung and T. Zhang, *Adv. Mater.*, 2015, **28**, 1668–1674.
- 8 B. Y. Xia, Y. Yan, N. Li, H. B. Wu, X. W. Lou and X. Wang, *Nat. Energy*, 2016, **1**, 15006.
- 9 P. Su, H. Xiao, J. Zhao, Y. Yao, Z. Shao, C. Li and Q. Yang, *Chem. Sci.*, 2013, **4**, 2941–2946.
- 10 H. Fei, J. Dong, M. J. Arellanojiménez, G. Ye, N. D. Kim, E. L. G. Samuel, Z. Peng, Z. Zhu, Q. Fan and J. Bao, *Nat. Commun.*, 2015, **6**, 8668.
- 11 P. Pachfule, D. Shinde, M. Majumder and Q. Xu, *Nat. Chem.*, 2016, **8**, 718–724.
- 12 J. Su, Y. Yang, G. Xia, J. Chen, J. Peng and Q. Chen, *Nat. Commun.*, 2017, **8**, 14969.
- 13 J. Wang, Z. Huang, W. Liu, C. R. Chang, H. Tang, Z. Li, W. Chen, C. Jia, T. Yao and S. Wei, *J. Am. Chem. Soc.*, 2017, **139**(48), 17281–17284.
- 14 D. He, K. Cheng, T. Peng, M. Pan and S. Mu, *J. Mater. Chem. A*, 2013, **1**, 2126–2132.
- 15 W. Liu, L. Zhang, W. Yan, X. Liu, X. Yang, S. Miao, W. Wang, A. Wang and T. Zhang, *Chem. Sci.*, 2016, **7**, 5758–5764.
- 16 P. Yin, T. Yao, Y. Wu, L. Zheng, Y. Lin, W. Liu, H. Ju, J. Zhu, X. Hong and Z. Deng, *Angew. Chem., Int. Ed.*, 2016, **55**, 10800–10805.
- 17 P. He, X. Y. Yu and X. W. Lou, *Angew. Chem., Int. Ed.*, 2017, **56**, 3897–3900.
- 18 G. Huang, F. Zhang, X. Du, Y. Qin, D. Yin and L. Wang, *ACS Nano*, 2015, **9**, 1592–1599.
- 19 Q. Lai, L. Zheng, Y. Liang, J. He, J. Zhao and J. Chen, *ACS Catal.*, 2017, **7**, 1655–1663.
- 20 B. You, N. Jiang, M. Sheng, W. S. Drisdell, J. Yano and Y. Sun, *ACS Catal.*, 2015, **5**, 7068–7076.
- 21 J. Meng, C. Niu, L. Xu, J. Li, X. Liu, X. Wang, Y. Wu, X. Xu, W. Chen and Q. Li, *J. Am. Chem. Soc.*, 2017, **139**, 8212–8221.
- 22 W. Zhang, X. Jiang, X. Wang, Y. V. Kaneti, Y. Chen, J. Liu, J. S. Jiang, Y. Yamauchi and M. Hu, *Angew. Chem., Int. Ed.*, 2017, **56**, 8435–8440.
- 23 L. Shang, T. Bian, B. Zhang, D. Zhang, L. Z. Wu, C. H. Tung, Y. Yin and T. Zhang, *Angew. Chem., Int. Ed.*, 2014, **53**, 250–254.
- 24 P. Hu, J. Zhuang, L. Y. Chou, H. K. Lee, X. Y. Ling, Y. C. Chuang and C. K. Tsung, *J. Am. Chem. Soc.*, 2014, **136**, 10561–10564.
- 25 Z. Qi, C. Xiao, C. Liu, T. W. Goh, L. Zhou, R. V. Maligalanes, Y. Pei, X. Li, L. A. Curtiss and W. Huang, *J. Am. Chem. Soc.*, 2017, **139**, 4672–4768.
- 26 J. L. Blin and B. L. Su, *Langmuir*, 2002, **18**, 5303–5308.
- 27 Z. Teng, X. Su, Y. Zheng, J. Zhang, Y. Liu, S. Wang, J. Wu, G. Chen, J. Wang and D. Zhao, *J. Am. Chem. Soc.*, 2015, **137**, 7935–7944.
- 28 Z. Kou, T. Meng, B. Guo, I. S. Amiinu, W. Li, J. Zhang and S. Mu, *Adv. Funct. Mater.*, 2016, **27**, 1604904.
- 29 I. S. Amiinu Ibrahim Saana Amiinu, Z. Pu, X. Liu, K. A. Owusu, H. G. R. Monestel, F. O. Boakye, H. Zhang and S. Mu, *Adv. Funct. Mater.*, 2017, **27**, 1702300.

- 30 D. He, L. Zhang, D. He, G. Zhou, Y. Lin, Z. Deng, X. Hong, Y. Wu, C. Chen and Y. Li, *Nat. Commun.*, 2016, **7**, 12362.
- 31 Z. Li, R. Yu, J. Huang, Y. Shi, D. Zhang, X. Zhong, D. Wang, Y. Wu and Y. Li, *Nat. Commun.*, 2015, **6**, 8248.
- 32 B. You, N. Jiang, M. Sheng, S. Gul, J. Yano and Y. Sun, *Chem. Mater.*, 2015, **27**, 7636–7642.
- 33 Y. Dai, B. Lim, Y. Yang, C. M. Cobley, W. Li, E. C. Cho, B. Grayson, P. T. Fanson, C. T. Campbell and Y. Sun, *Angew. Chem., Int. Ed.*, 2010, **49**, 8165–8168.